Supporting Information

4D Printing of Extrudable and Degradable Poly(Ethylene Glycol) Microgel Scaffolds for Multidimensional Cell Culture

*Connor E. Miksch, Nathaniel P. Skillin, Bruce E. Kirkpatrick, Grace K. Hach, Varsha V. Rao, Timothy J. White, Kristi S. Anseth**

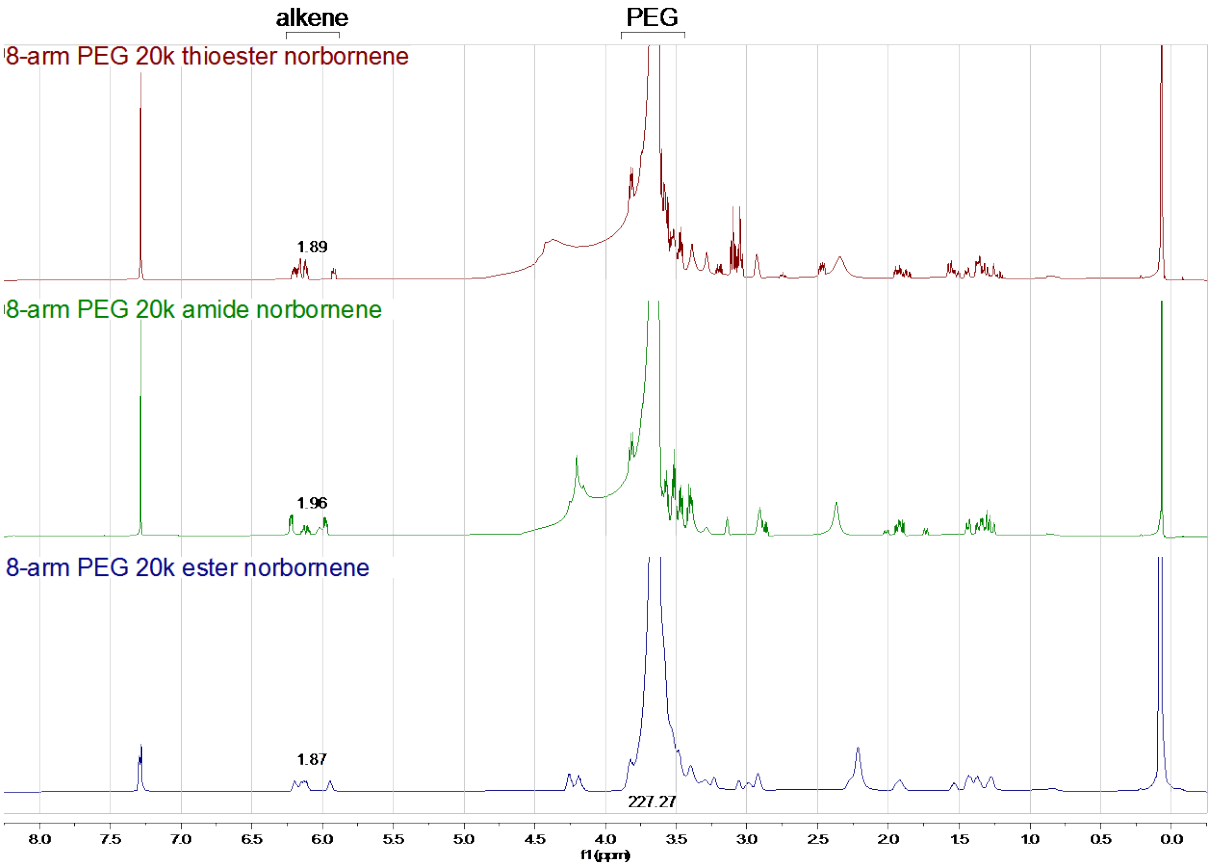

Figure S1. ^{1}H NMR analysis of 8-arm 20 kDa PEG-norbornene macromers.

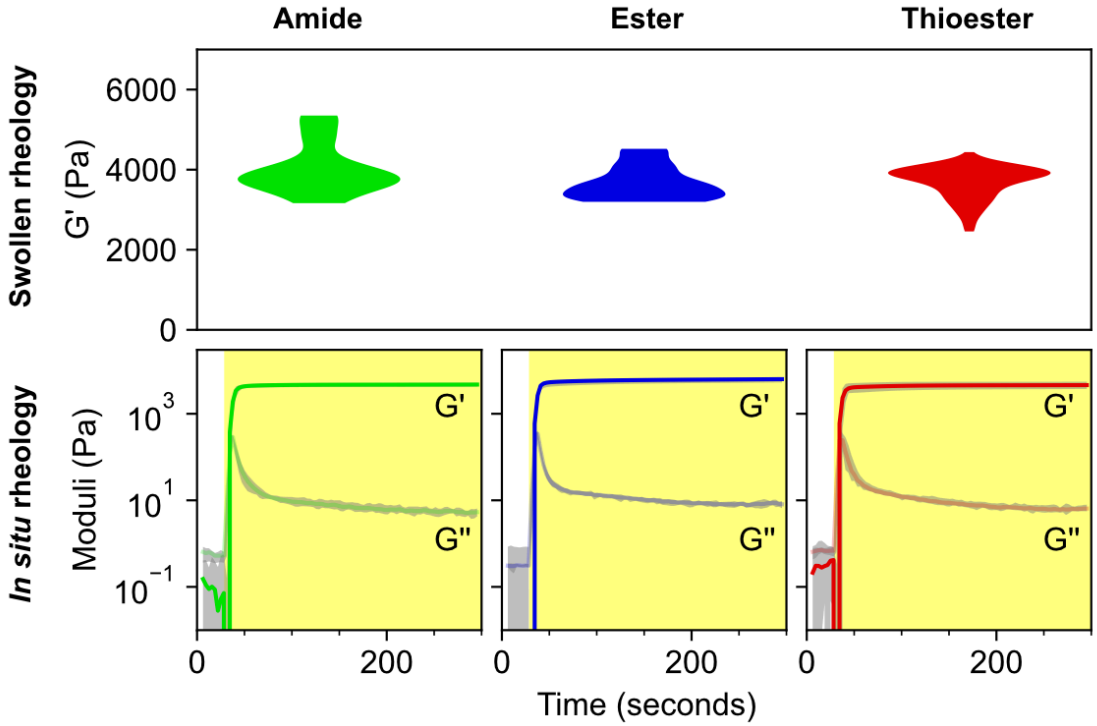

Figure S2. Oscillatory shear rheology of *in situ* and swollen bulk hydrogel (amide, ester, and thioester-linked macromers) photocrosslinking.

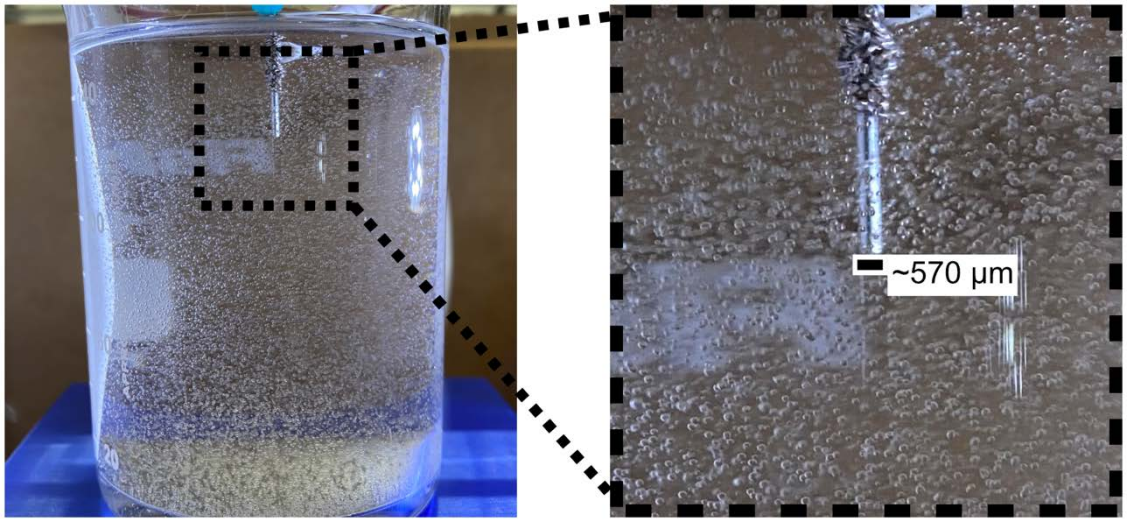

Figure S3. Electrospray generates in excess of 10^5 microgels within minutes.

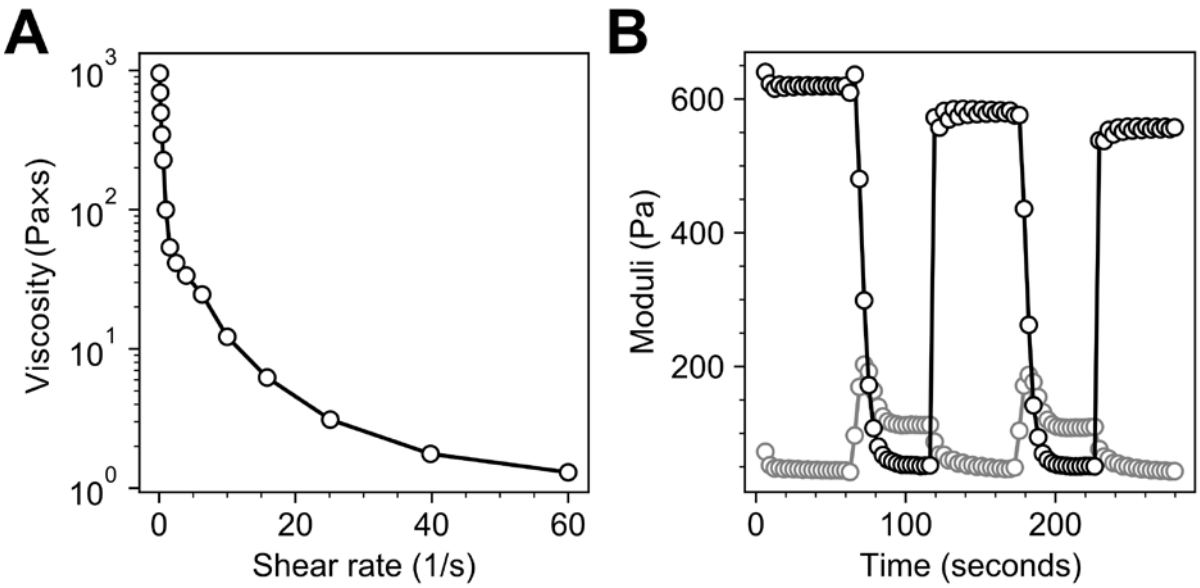

Figure S4. Printability of unannealed jammed microgels. A) Viscosity-shear rate relationship shows classical shear-thinning behavior for granular bioinks. B) Oscillating between low (0.1%) and high (300%) strain shows crossover between storage (black) and loss (grey) moduli and recovery.

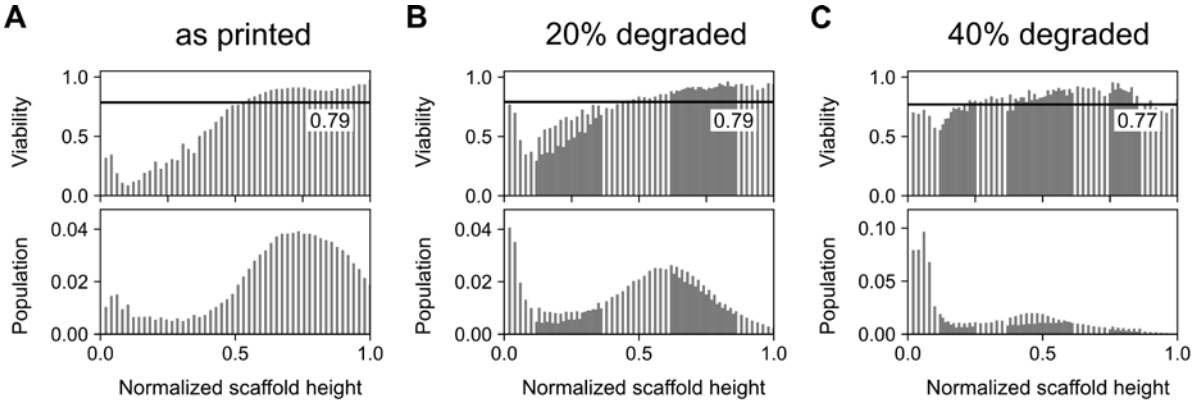

Figure S5. A-C) Day 7 viability and population distribution in 0%, 20%, and 40% degraded amide-linked microgel scaffolds. Bin widths for population data were ~0.02.

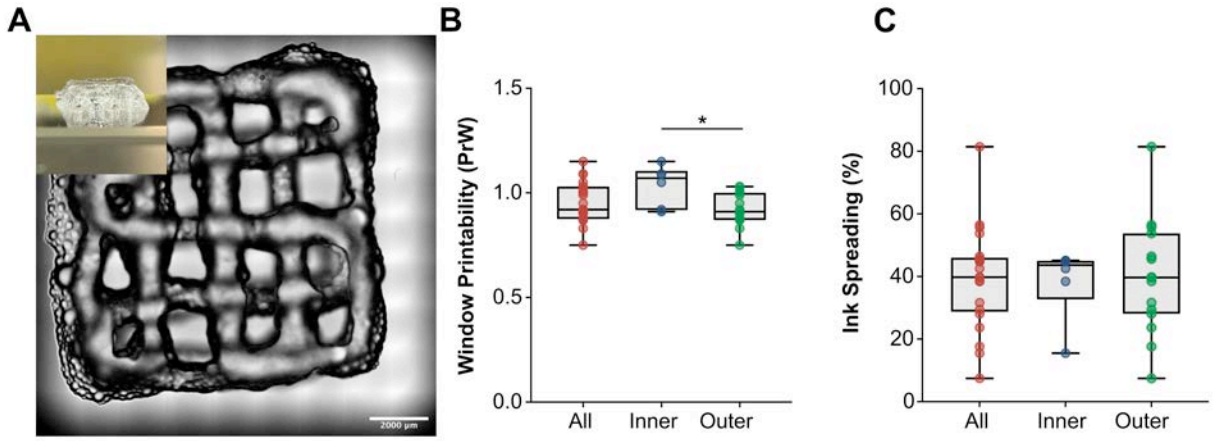

Figure S6. Assessment of microgel printing fidelity using a previously demonstrated method.[18a] A) Brightfield microscope image of 3D printed 10mmx10mm lattice structure using PEG-amide microgels (scale bar = 2000 μm). Lattice was printed with an 18 gauge tapered tip needle at 2mm/s with 4 layers (layer height = 800μm). B) Quantification of ink spreading (Sp) and C) window printability (Pr_w). Data is plotted as a box and whisker plot, with whiskers showing the minimum and maximum values, with each window plotted as a single point. (n = 21 windows, two independent prints). Inner windows had significantly greater window printability compared to outer windows (p=0.0124, unpaired t-test), illustrating approximation of printed filament and nozzle path when attempting 90˚ turns and potential for optimization of GCode to match inner windows if greater fidelity is required.

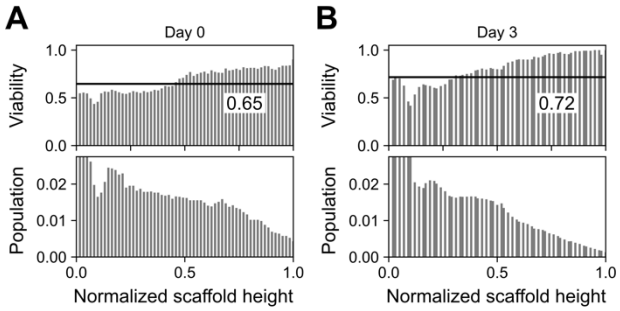

Figure S7. Cell viability and population distributions throughout bioprinted and annealed scaffolds comprised of amide microgels A) immediately following extrusion and B) after three days of culture. Lower viability is attributed to overjamming resulting in excessive

drying and shear, as well as non-sterile print conditions. Bin widths for both histograms are ~0.015.

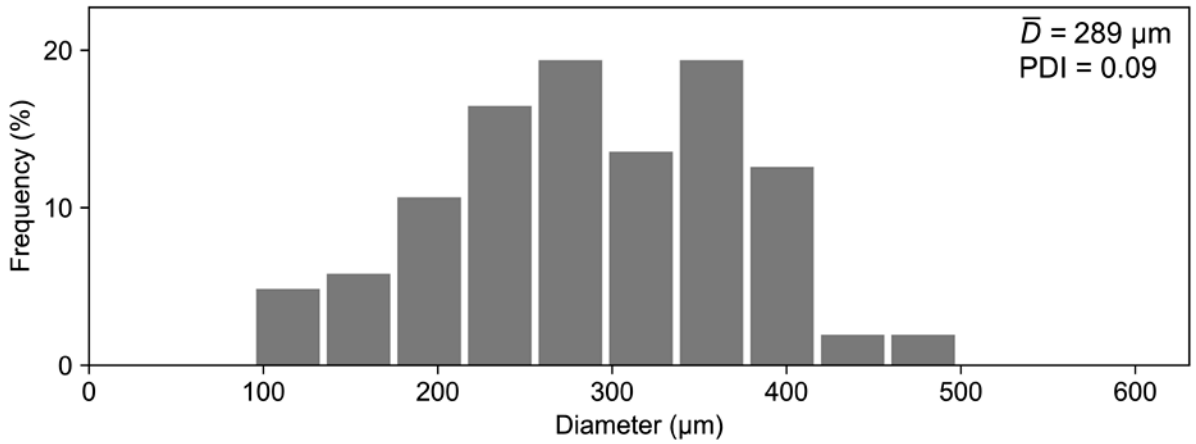

Figure S8. MMP-labile peptide-linked microgels are slightly larger than PEG-thiol-linked microgels but have similar polydispersity.

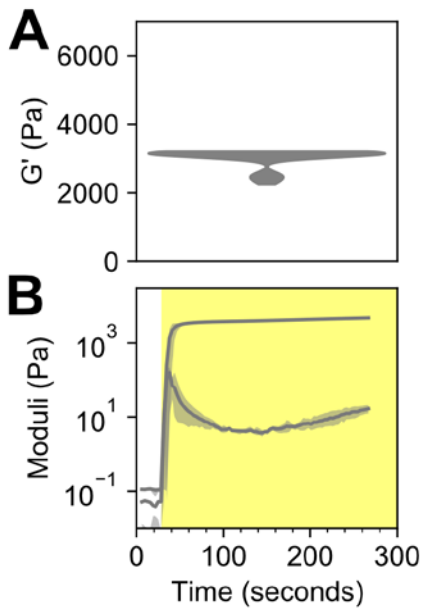

Figure S9. Oscillatory shear rheology of A) swollen and B) *in situ* bulk MMP-peptide-linked hydrogel photocrosslinking.

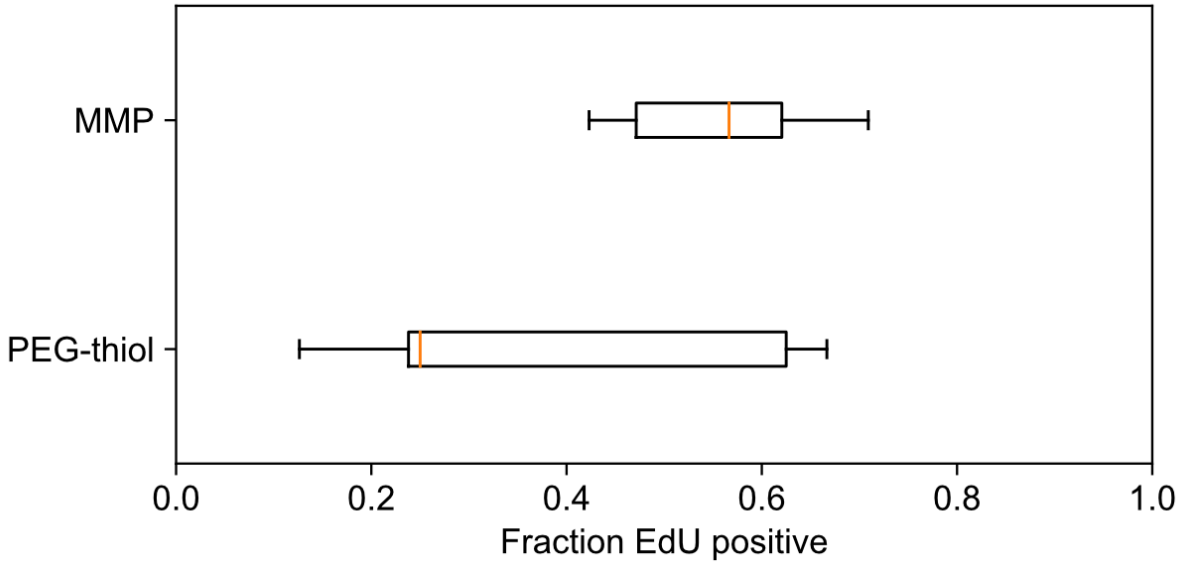

Figure S10. Cells cultured in 2.5D on MMP-peptide-linked microgels are more proliferative at day 7 than PEG-thiol-linked controls (as measured by EdU assay).

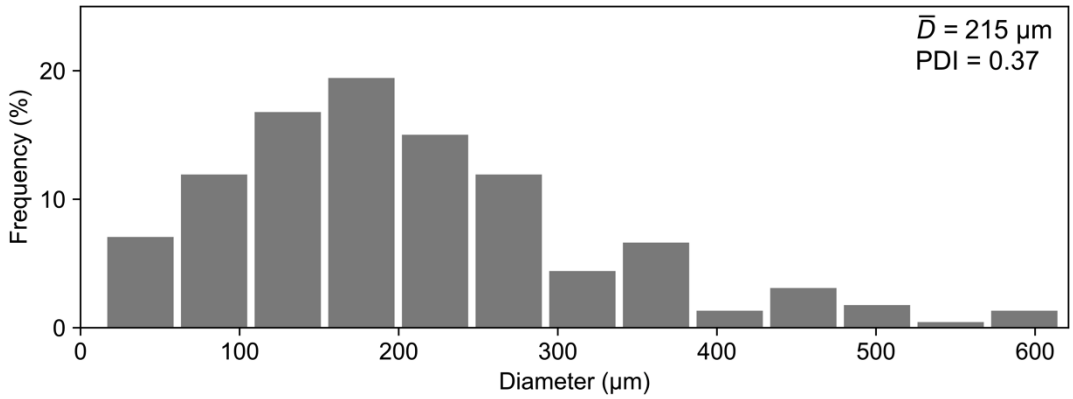

Figure S11. Cell-encapsulating microgels are of comparable size to but are more polydisperse than non-encapsulating microgels.

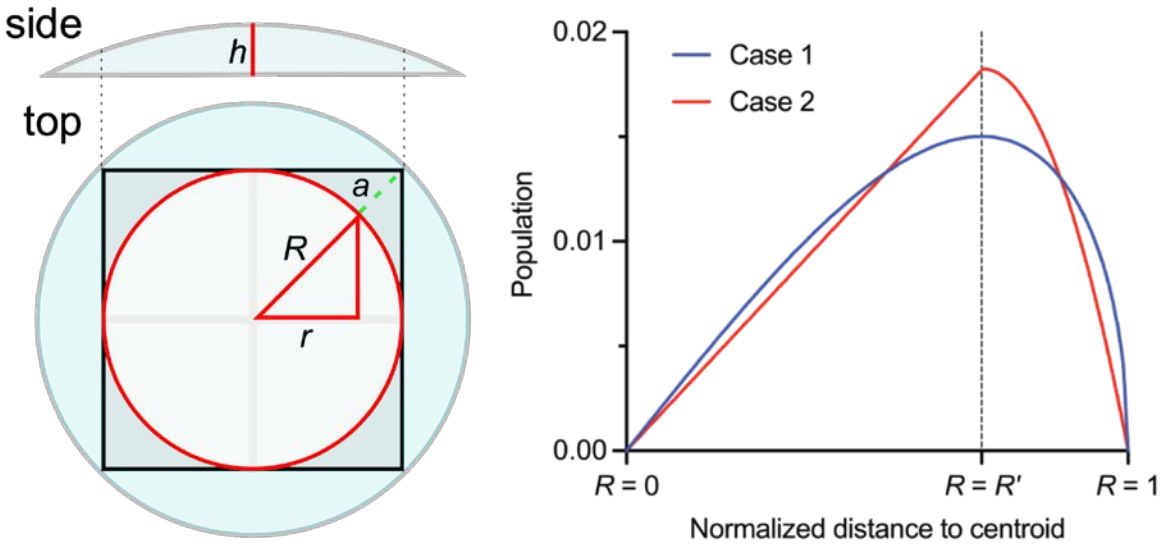

Figure S12. Modeling a homogeneously distributed population of cells through a dome-shaped scaffold (imaged in a square ROI). Note that these cases assume that the radius of our microgel scaffolds is equal to 1 (i.e., normalized distance to centroid).

Case 1 (3D, scaling by swept area of cylinder expanding radially from center of dome):

$$h = \sin(\text{acos}(R)), 0 \leq R \leq 1$$

$$c = 2\pi R, 0 \leq R \leq 1$$

$$A = h * c$$

A is then normalized to an AUC of 1.

Case 2 (2D, scaling by circumference normalized to projected area of circle expanding radially from center of disc):

Here, the circumference of the circle inlaid within the square ROI spanning the diameter of the disc-shaped scaffold can expand linearly until its radius equals half the height of the square (this is illustrated in the schematic). As *R* increases beyond this value, the "projected circumference" (from the upper to lower surface of the dome-shaped scaffold) is approximated as decreasing at a rate scaled to the proportion of volume remaining in an inlaid circle of radius *a*.

The radial value at which this occurs, or *R'*, is the hypotenuse length of an isosceles right triangle that extends to a circle inscribed within a square with side lengths = 1:

$$2R' = \sqrt{2 * 1^2} \rightarrow R' \approx 0.71$$

$$c = 2\pi R, 0 \leq R \leq R'$$

$$c' = 2\pi R'$$

$$a = 1 - R'$$

$$c = c'\left(1 - \left[\frac{\mathrm{abs}(1 - R - a)}{a}\right]^2\right), R' \leq R \leq 1$$

c is then normalized to an AUC of 1. We found that Case 2 better describes our data and used this approach to describe a homogenous distribution of cells in these scaffolds. Regardless, both cases identify a local maximum in the radial measurement of cell frequency as a function of distance from the centroid at $R' = 2^{-1/2}$ and describe the profile of the cell distribution in our scaffolds relatively well.

Movie S1. Taylor cone formation during electrospray startup. Scale is the same as Figure S3. Nozzle outer diameter is ~570 µm.
Movie S2. Extrusion bioprinting of microgels on Bio-X and Hyrel printers. Videos are played at 2X speed. For scale, 18-gauge extrusion tip has an inner diameter of ~840 µm.
Movie S3. Volumetric reconstruction of printed scaffold void space (degraded fraction = 0.2). Scale bar = 500 µm.
Movie S4. Volumetric reconstruction of series and parallel microgel scaffold degradation. Each video represents several hours of recording. Microgel scale is same as in Figure 3.
Movie S5. Volumetric reconstruction of cell-encapsulating microgel, which is ~250 µm in diameter.